

Size effect on seismic performance of high-strength reinforced concrete columns subjected to monotonic and cyclic loading



Zhenbao Li^a, Chunyi Yu^a, Yongping Xie^{b,*}, Hua Ma^a, Zhenyun Tang^a

^a The Key Laboratory of Urban Security and Disaster Engineering, Ministry of Education, Beijing University of Technology, Beijing 100124, China

^b College of Exploration Technology and Engineering, Hebei GEO University, Shijiazhuang 050031, China

ARTICLE INFO

Keywords:

Size effect
Seismic performance
High-strength reinforced concrete columns
Factor of safety
Local factor of safety
Moment capacity

ABSTRACT

It has been shown that as concrete strength increases, the size effect becomes more pronounced in both samples and members. However, the effect of section size on the seismic performance of high-strength reinforced concrete columns requires further confirmation. For this purpose, six high-strength reinforced concrete columns were subjected to monotonic and cyclic loading in this study. The experimental results indicate that the relative nominal flexural strength, average energy dissipation coefficient, factor of safety, and local factor of safety all exhibited a strong size effect by decreasing as the column size increased. Moreover, the size effect on the factor of safety was stronger for high-strength columns than for conventional columns. The observed changes in the factor of safety were in good agreement with the Type 2 size effect model proposed by Bažant; so, using the local factor of safety and Bažant's Type 2 model, the code equation for moment capacity was modified to provide a constant factor of safety regardless of column size.

1. Introduction

As the scale of engineering structures increases, the safety of their larger components has become one of the primary topics of concern, especially when taking into account the use of high-strength concrete [1]. The size effect, defined as the change in structural behavior with changing size rather than material, though not yet captured by the conventional design process, is increasingly accepted in theory [2–10]. Indeed, a large number of experimental results have demonstrated that the size effect exists in plain concrete samples and structural concrete components, such as plain concrete columns [11,12], reinforced concrete (RC) beams [13–15], RC columns [16–18], and RC beam-column joints [19–20]. Moreover, the size effect has been found to be more significant in high-strength concrete than in conventional concrete [1,12,21,22], but the size effect on the seismic performance of high-strength RC columns remains to be determined.

In this study, the classical model of the size effect law was first investigated so that the correct theoretical model could be applied to a structural design. The scaling problem of primary interest is the effect of a structure's size on its nominal strength [2]. The structural ultimate load predicted by any deterministic strength theory (e.g. the elastic, plastic, or elastoplastic strength criteria) applied to ductile materials exhibits no size effect. In 1921, Griffith [3] proposed linear elastic fracture mechanics (LEFM) and introduced fracture mechanics into the

study of size effect. For brittle, geometrically similar structures, linear elastic fracture mechanics shows that nominal strength decreases as structure size increases, following the trend of an inclined asymptote with a slope of $-1/2$. Then Weibull [4,5] derived an equation capturing the size effect on mean structural strength based on the Weibull distribution. This approach is certainly valid for various fine-grain ceramics and for metal structures embrittled by fatigue. Bažant identified the Type 1 size effect [2,8], the Type 2 size effect [6], and the universal size effect law [9]. These laws are suitable for quasi-brittle materials, such as plain concrete samples and components, whose properties are between those of ductile and brittle materials. In recent research, Hoover and Bažant [10] established an improved universal size effect model. Considering the absence or presence of a statistical size effect, the improved universal size effect model is divided into two types: the Type 1 size effect is used for failures at crack initiation [2], such as in beams without stirrups, while the Type 2 size effect occurs in notched fracture specimens or in structures that fail only after the stable growth of large cracks [2]. However, when a crack is no longer than the length of the fracture process zone (FPZ), an improved universal size effect law between Type 1 and Type 2 can be applied, as the length of a macroscopic crack can't be neglected, and should not reach the length of the FPZ [23]. The relationship between these various size effect models has been described in the literature [23]. The applicable conditions for the different types of size effect models are shown in Fig. 1.

* Corresponding author.

E-mail addresses: lizb@bjut.edu.cn (Z. Li), 15710061307@163.com (C. Yu), axypa@163.com (Y. Xie), mahua@bjut.edu.cn (H. Ma), tzy@bjut.edu.cn (Z. Tang).

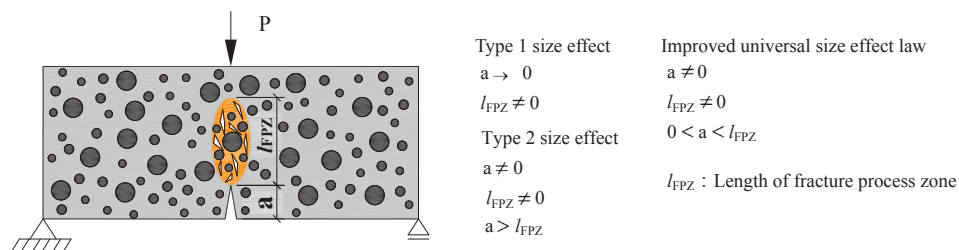


Fig. 1. Applicable conditions for different types of size effect models.

Table 1
Mix proportions of concrete.

Grade number	Water [kg/m ³]	Cement [kg/m ³]	Sand [kg/m ³]	Gravel [kg/m ³]
C60	158	395	672	1051

Under earthquake loading, flexural failure, shear failure, and flexure-shear failure occur in a large number of larger-sized components, such as piers, frame columns at the bottom of a story, and short columns. The Wenchuan earthquake in China (2008) demonstrated all of these phenomena [24,25]. Accordingly, Li et al. [26,27] and Xie et al. [28] investigated the effect of different member sizes on the seismic performance of conventional RC columns subjected to monotonic and cyclic loading. It was found that the relative nominal flexural strength, average energy dissipation coefficient, and factor of safety all decreased as the section size increased, suggesting a strong size effect. However, less work has been done to systematically assess the impact of the size effect on the seismic performance of high-strength RC columns. Li et al. [1], Su et al. [12], and Koç et al. [21] found that the nominal strength of plain concrete samples and members decreased with the increase in section size, and that with increasing concrete strength, the size effect became more pronounced, which suggests that high-strength concrete would exhibit a pronounced size effect. Indeed, El-Sayed [22] found that the size effect in high-strength concrete deep beams was greater than that in conventional concrete deep beams.

Several studies have analyzed the factors affecting the seismic performance of high-strength reinforced concrete columns. These factors were mainly the concrete strength, yield strength of the stirrups, applied axial load, volume-stirrup ratio, and confinement. Results indicated that increasing the concrete compressive strength resulted in a reduction in ductility [29]. Others [30,31] have found that increasing the yield strength of the stirrups had little influence on the ductility and dissipated energy at axial loads below 30% of capacity. However, use of high yield-strength steel as stirrups has been found to be beneficial when the applied axial loads are relatively high—above 40% of capacity [32]. Additionally, the ductility and dissipated energy have been observed to increase as the volume-stirrup ratio increased, but they decreased as the applied axial load increased [33–35]. With respect to the effects of confinement, Wang et al. [36] found that bonded carbon fiber-reinforced polymer (CFRP) wraps placed at potential hinge regions could improve the ductility and energy dissipation capacity of high-strength concrete columns subjected to high axial loads. Notably, however, little work on the seismic performance of concrete columns has accounted for the size effect. Indeed, the size effect in high-strength RC columns under seismic action has been rarely reported.

In this study, high-strength RC columns were subjected to monotonic and cyclic loading. Based on a combined experimental analysis, the failure mechanisms of these columns when constructed in different structural sizes were studied, the size effect rule for different mechanical parameters was obtained, and the impact of the size effect on the seismic behavior of high-strength RC columns was determined. In total, six high-strength RC columns were investigated experimentally, in which the sizes of the materials and components were kept

geometrically proportional. The section sizes of the tested specimens were 300, 500, and 700 mm, and the column lengths were 1092, 1820, and 2548 mm.

2. Experimental program

2.1. Material properties

The mixture proportions of the concrete used in this study are summarized in Table 1. The type of cement was P42.5 Portland cement, and the mix consisted of medium sand as the fine aggregate (an average diameter of 2.7 mm) and crushed pebble stones as the coarse aggregate (an average diameter between 5 mm and 25 mm). The slump of the concrete was 160 ± 20 mm. The material properties of concrete are listed in Table 2. When tested according to the Chinese standards for the mechanical properties of concrete (GB/T 50081-2002) [37], the average compressive strength of the standard 150-mm cubic concrete samples was 67.98 MPa, the average compressive strength of the standard $150 \times 150 \times 300$ mm prismatic concrete samples was 49.67 MPa, and the average tensile strength of the standard 150-mm cubic concrete samples was 3.76 MPa.

The material properties of the steel rebar used in the test specimens are listed in Table 3. The material properties, including yield strength, ultimate tensile strength, and modulus of elasticity, were determined by rebar tests according to the Chinese standard for determining the mechanical properties of steel (GB/T 228.1-2010) [38].

2.2. Specimen description

The selected column cross sections were 300, 500, and 700 mm square, and the longitudinal bar size and spacing, stirrup size, and thickness of concrete cover of each specimen were scaled proportionally to the column cross section. The details of the specimens and bars are provided in Table 4, along with an explanation of test specimen nomenclature. Reinforcement details and column dimensions are shown in Fig. 2.

2.3. Loading apparatus and loading scheme

2.3.1. Loading apparatus

A total of six high-strength RC columns of three different structural sizes were investigated experimentally. The 300-mm specimens were tested using small range actuators (shown in Fig. 3(a)) that provided vertical and horizontal maximum loads of 2000 kN and 500 kN, respectively. However, because the axial compressive strengths of the other specimens were considerably larger, the loading apparatus in Fig. 3(a) could not provide sufficient axial load. As a result, the 500-

Table 2
Material properties of concrete.

Grade number	Prismatic specimen size [mm ³]	f_{ik} [MPa]	f_{ck} [MPa]
C60	$150 \times 150 \times 300$	3.67	49.67

Table 3
Material properties of steel reinforcing bar.

Bar size [mm]	Bar grade	Yield strength [MPa]	Ultimate strength [MPa]	Modulus of elasticity [MPa]	Yield strain ($\times 10^{-6}$)
6	HPB300	441	690	251,657	1752
10	HPB300	346	501	197,265	1779
14	HPB300	351	490	199,279	1736
12	HRB400	478	625	196,752	2429
20	HRB400	451	595	195,233	2310
28	HRB400	455	636	191,655	2374

Note: HPB indicates plain reinforcement and HRB indicates deformed bar reinforcement.

and 700-mm specimens were tested in a slightly different configuration using more powerful small range actuators (as shown in Fig. 3(b)) that provided vertical and horizontal maximum loads of 40,000 kN and 4000 kN, respectively. The axial load was provided by the vertical actuator, and the horizontal load was provided by the horizontal actuator. Displacement was measured using an LVDT in the locations shown in Fig. 3, and the indicated H_0 was used as the theoretical height of the column in later calculations. Fig. 4 depicts the application of force and the resulting deformation characteristics of the specimens, in which F is the horizontal force; N is the vertical force; f_y and f'_y are the yield strengths of the longitudinal tensile and compressive rebar, respectively; σ_s and σ'_s are the stresses in the longitudinal tensile and compressive rebar, respectively; and σ_c is the concrete compressive stress at the edge of the column. Fig. 5 depicts the geometry of all column specimens subjected to axial compression and shear loads.

2.3.2. Loading scheme

The column specimens were subjected to a combination of vertical and horizontal loading. The horizontal load simulated the effect of seismic action in the form of monotonic and cyclic loading, while the vertical load applied by the actuator was held constant at an axial load ratio of 0.4 for the entire test as the specimen was loaded horizontally until failure. The load-displacement hybrid control method was adopted in the loading system: prior to specimen yielding, the load was applied in load increments, while after yielding, the load was applied in displacement increments. The development of various failure modes of the specimens was intermittently recorded during the entire loading process.

For the columns subjected to monotonic and cyclic loading, the horizontal load was applied to the columns at 20, 40, 60, 80, and 100% of the yield load. After reaching the yield load, the displacement at yield, Δ_y , was used to set the applied horizontal displacement control load in multiples, i.e. Δ_y , $1.5\Delta_y$, $2\Delta_y$, $2.5\Delta_y$, ..., $n\Delta_y$, until failure, defined as the decrease in the apparent load capacity to 85% of the maximum supported load [39]. For specimens subjected to cyclic loading, one cycle was applied at each pre-yield load level and two cycles were

Table 4
Details of specimens and bars.

Test no.	b [mm]	h [mm]	H [mm]	f_{ck} [MPa]	Concrete cover [mm]	λ	Stirrup	Longitudinal bar	ρ [%]	ρ_{sv} [%]
WD-3	300	300	1092	49.67	15	4.00	4A6@43	12C12	0.55	0.88
WD-5	500	500	1820 + 300	49.67	25	4.66	4A10@71	12C20	0.55	0.88
WD-7	700	700	2548 + 300	49.67	35	4.47	4A14@100	12C28	0.55	0.88
WF-3	300	300	1092	49.67	15	4.00	4A6@43	12C12	0.55	0.88
WF-5	500	500	1820 + 300	49.67	25	4.66	4A10@71	12C20	0.55	0.88
WF-7	700	700	2548 + 300	49.46	35	4.47	4A14@100	12C28	0.55	0.88

Note: WD and WF represent flexural components subjected to monotonic and cyclic loading, respectively, while the number following represents the cross sectional dimensions of the specimen in hundreds of mm; b and h represent the cross sectional dimensions; H represents the total height of the column and spherical hinge (in which + 300 mm represents the additional spherical hinge height); f_{ck} represents the axial compressive strength of the concrete; λ is given by H/h_0 ; ρ is determined by $A_s/(bh_0)$, where A_s is the required tensile or compressive steel area and h_0 is the effective depth of the column; and ρ_{sv} is the ratio of stirrup area to column area given by $A_{sv}/(bs)$, where A_{sv} is the area of the stirrup, and s is the stirrup spacing.

applied at each post-yield displacement level. The loading scheme is plotted in Fig. 6.

2.3.3. Arrangement of strain gages

The strains in the longitudinal bars and stirrups were measured with strain gages at the locations shown in Fig. 7. Then the stress-strain relationship of the steel was used to compute the bar stresses to verify the force in and deformation of the specimens. For longitudinal bars, there were five levels of strain gages along the column height, and for stirrups, there were two levels.

3. Test results and discussion

3.1. Failure modes

(1) Monotonic specimens

The development of the failure modes of the monotonic specimens are shown in Fig. 8 at three stages: yield load, maximum load, and failure load. First of all, note that the characteristics of the flexure-shear cracks of different size specimens are similar. A horizontal crack occurs in the position of the maximum moment when the yield load is reached. Meanwhile, there are flexure-shear cracks with shallow angles in the upper portion of the specimens. The angle of the flexure-shear cracks reaches its maximum of 45 degrees when the maximum load is reached. At the failure load, the flexure-shear cracks continue to extend and widen, but their general shape and number no longer change. After failure, there were generally between four and five flexure-shear cracks on each specimen, each with a horizontally projected length approximately equal to half the column width. Similarly, the development of vertical splitting cracks in different size specimens was similar. A vertical splitting crack was first produced in the compression zone when the yield load was reached. Once the maximum load was reached, more obvious vertical splitting cracks were produced. Then, when the failure load was reached, the vertical splitting cracks widened, extended upward, and developed into the neutral axis. Finally, crushing of the concrete was observed in compressive zone at failure.

(2) Cyclic specimens

The development of the failure modes of the cyclic specimens are shown in Fig. 9, also for three stages: yield load, maximum load, and failure load. As the applied load increased, the angle of the flexure-shear cracks increased. When the load reached its maximum value, the angle of the flexure-shear cracks was also approximately 45 degrees. Once the failure load was reached, the horizontally projected lengths of the curved shear cracks were approximately equal to half the column width. At the same time, the positive and negative flexure-shear crack geometries were symmetrical. There were roughly four or five flexure-shear cracks at failure, the same as in the monotonic specimens. The vertical splitting cracks also developed in a fashion similar to the monotonic specimens: with the increase in load, the length and number of vertical splitting cracks increased. Finally, the concrete in the

Length unit: mm

Axial load ratio: 0.4

Grade of concrete: C60

Grade of stirrup: HPB300

Grade of longitudinal bar: HRB400

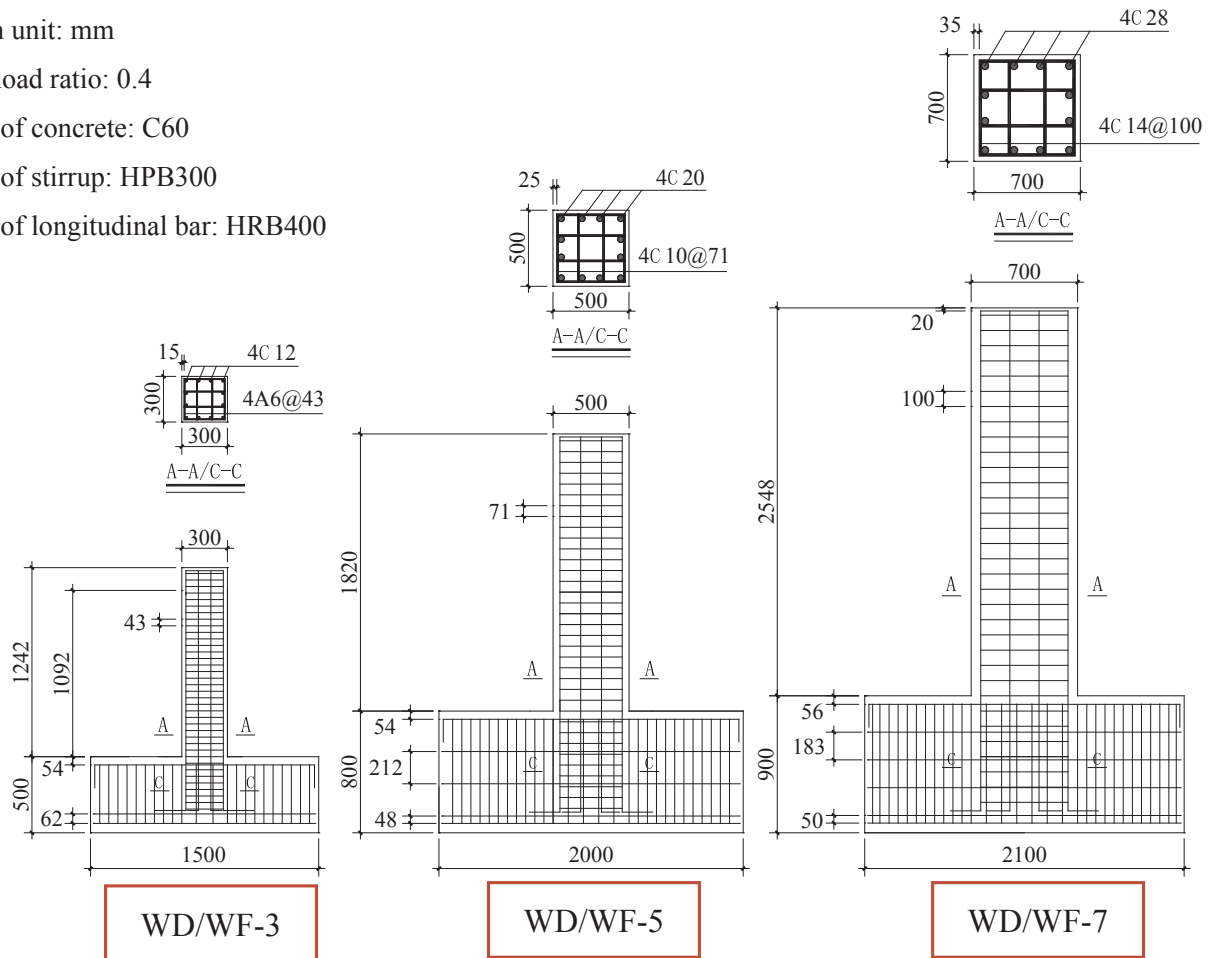


Fig. 2. Details of the tested RC columns.

compression zone was also observed to crush at failure.

In summary, the failure modes of the monotonic and cyclic specimens were found to develop in a similar manner consistent with the flexural failure process. Moreover, the failure region was mainly concentrated in the plastic hinge zone at the column foot. The obvious vertical splitting crack, located in the concrete cover, is a manifestation of the brittleness of high-strength concrete. This crack may be caused by the splitting effect of the stirrup and longitudinal bar combined with the

repeated tension and compression stress in the concrete. It is important to note here that the brittle splitting of high-strength concrete is different from that of ordinary concrete [26,28], which has a longer splitting length. Generally, for both the monotonic and cyclic specimens, large stable crack growth was observed before reaching the maximum load [2], which is in accordance with Bažant’s Type 2 size effect model [6]. Foraboschi [40,41] found that a critical crack length was eventually reached, causing external fiber-reinforced polymer

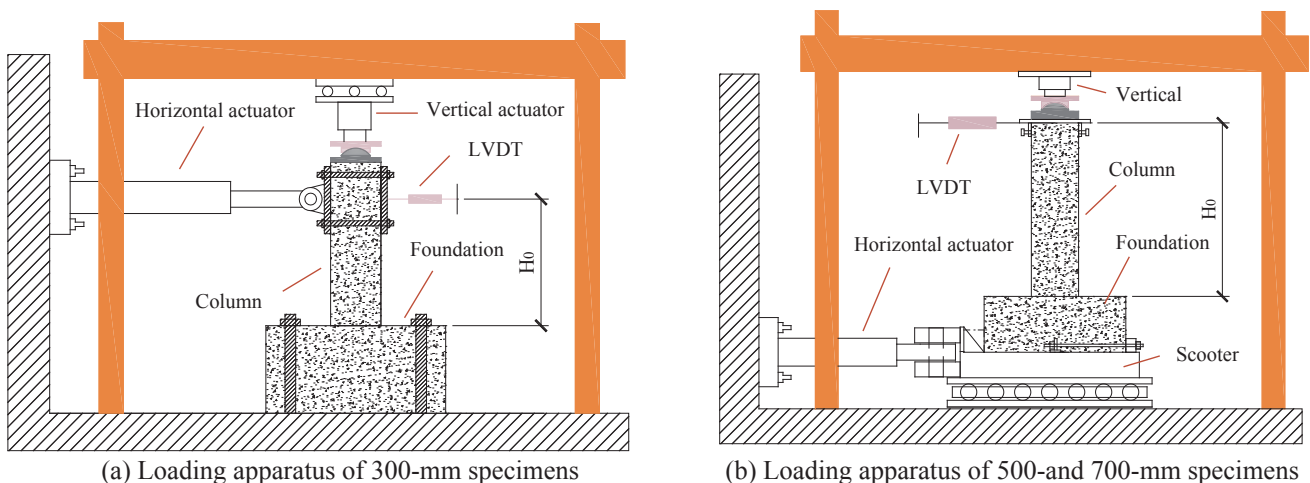


Fig. 3. Loading apparatus for all specimens.

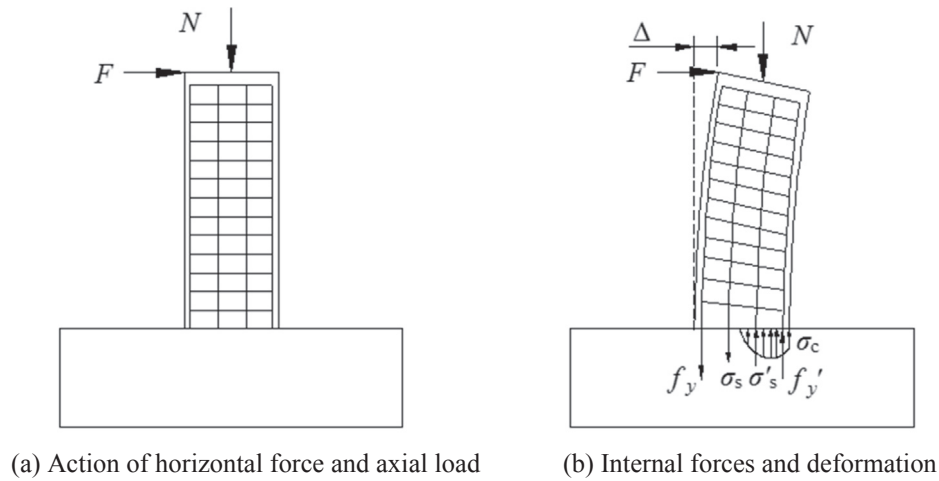


Fig. 4. Schematic of applied force and resulting deformation for all specimens.

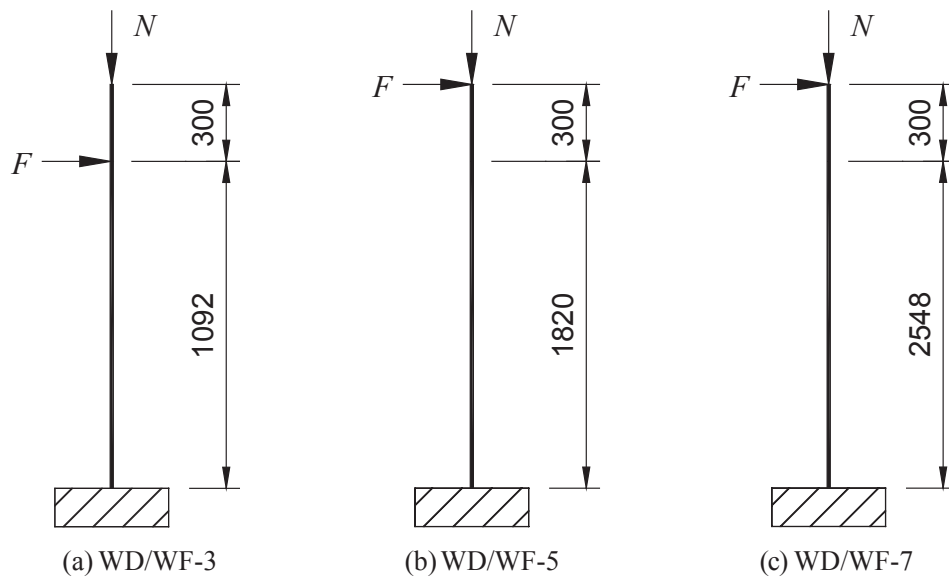


Fig. 5. Calculation diagram of force for all specimens.

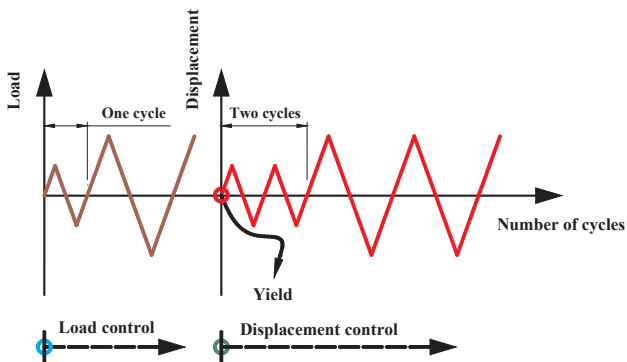


Fig. 6. Loading scheme for cyclic specimens.

(FRP) reinforcement installed on the specimen to lose its bond due to the effect of existing cracks whose major axis were parallel to the axis of the beam. Thus, existing cracks may also affect the vertical crack growth and concrete compressive strength particularly within the concrete cover of large-sized columns, which may constitute a size-related effect.

3.2. Horizontal load-displacement curves

(1) Monotonic specimens

Fig. 10 shows the relationship between force and deformation, in which the vertical axis represents the applied horizontal load and the horizontal axis represents the horizontal displacement between the top and bottom of the column. It was observed that the maximum bearing capacity of the specimen was affected by the sudden separation of the concrete cover from the core concrete in the large-sized specimens. Notably, the specimen behaviors exhibited only a short plateau at the maximum load. When evaluated together with the failure modes, this effect is obviously related to the development of the vertical splitting crack, indicating that the vertical splitting crack may be a factor influencing the size effect. Additionally, note that when the resisted load begins to decrease, the slope of the decreasing load is steeper with the increase in the specimen section size.

In Fig. 10 the initial cracking load of the specimens is not obvious, likely due to the influence of the axial load. Therefore, only the yield load, maximum load, and failure load are used as the characteristic points of the curve. The calculation of yield load and failure load is shown in Fig. 11. The yield point Y was determined by the equivalent elastic-plastic energy method, that is, where the area $BYC = OAB$, and

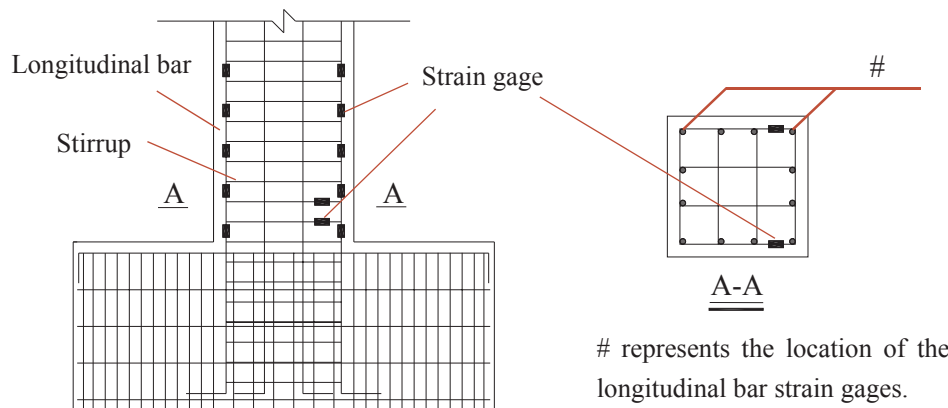


Fig. 7. Strain measurement points in the longitudinal bars and stirrups.

the failure load was simply defined as 85% of maximum load [39]. The calculated loads and displacements are shown in Table 5, indicating that the calculated yield load is between 85% and 88% of the maximum load. In the table, the variables P_y , P_m , and P_u indicate the yield load, maximum load, and failure load, respectively, while Δ_y , Δ_m , and Δ_u indicate the displacements at the yield, maximum, and failure loads, respectively.

(2) Cyclic specimens

The relationships between load and displacement for the cyclic specimens are shown in Fig. 12(a), (b), and (c), in which the vertical axis represents the applied horizontal load and the horizontal axis represents the horizontal displacement between the top and bottom of the column. The positive and negative loading and unloading curves of the specimens exhibit the following characteristics:

- (1) The areas of the hysteresis loops are small prior to the maximum load. When the specimens enter the softening stage, the areas of their hysteresis loops obviously increase, indicating that the energy dissipation capacity of the specimens is weakening.
- (2) The residual deformation is small prior to the maximum load. When the specimens are in the softening stage, the residual deformation obviously increases, indicating that the elasticity-plasticity of the component is stronger than earlier, and that the nonlinearity of the specimens increases gradually throughout the entire loading process, but especially during the softening stage.
- (3) The strength degradation of the specimens are basically constant during the entire loading process, so there is no obvious point of initiation. Additionally, the application of the second loading cycle passes through the first cycle load level, balancing the forces induced by the initial damage and causing the initial cracks to close and then reopen where they left off in the last cycle. This demonstrates that the degree of damage caused by cyclic loading is basically consistent throughout the loading process.

Based on the hysteresis curves, a skeleton curve can be obtained by taking the maximum load in the first loading cycle of every load level, as shown in Fig. 13, in which the vertical axis represents the applied horizontal load and the horizontal axis represents the horizontal displacement between the top and bottom of the column. It can be seen that this load-displacement skeleton curve is similar to the load-displacement curve of the monotonic specimens. There is also a short plateau in these curves, especially for the larger-sized specimens, reflecting the effect of the vertical splitting cracks on moment capacity, and thus these cracks should not be neglected, as they could be linked to the size effect.

For the cyclic specimens, the calculation of key load points was similar to that of the monotonic specimens. The resulting load and displacement values are given in Table 6, which shows that the calculated

yield load was between 86% and 88% of the maximum load. In the table, the variables P_y , P_m , and P_u indicate the yield load, maximum load, and failure load, respectively, while Δ_y , Δ_m , and Δ_u indicate the displacements at the yield, maximum, and failure loads, respectively.

3.3. Analysis of strain in longitudinal bars and stirrups

The strains in the longitudinal bars and stirrups of the monotonic and cyclic specimens are given in Table 7 and Table 8, respectively. The following characteristics were observed:

- (1) For the monotonic WD specimens, the strain in the longitudinal bars reached the yield strain, while the strain in the stirrups did not.
- (2) For the cyclic WF specimens, the strain in the longitudinal bars reached the yield strain, but only the stirrups in specimen WF-3 reached yield. Still, the overall strain in the stirrups was larger than for the monotonic specimens, indicating that the damage caused by cyclic action weakens the shear modulus of the specimens.

Generally, the overall mechanical behavior of the reinforcement was characterized by the strain in the longitudinal bars reaching the yield strain and the strain in the stirrups not, indicating that the likely final failure mode of the specimens would be in flexure before shear.

3.4. Effect of section size on seismic performance

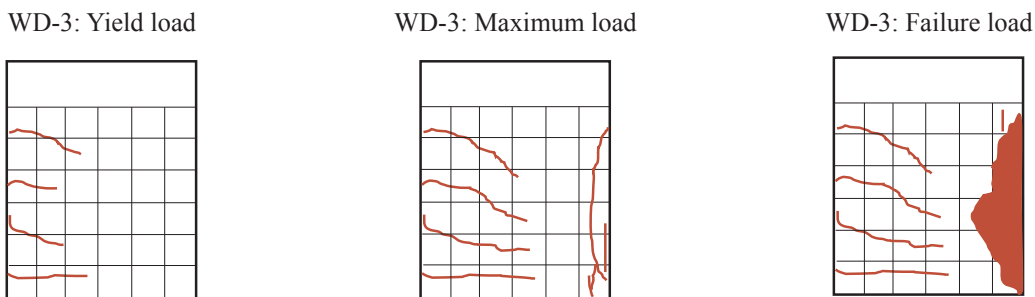
3.4.1. Relative nominal flexural strength

The ultimate moment considering the second-order effect is

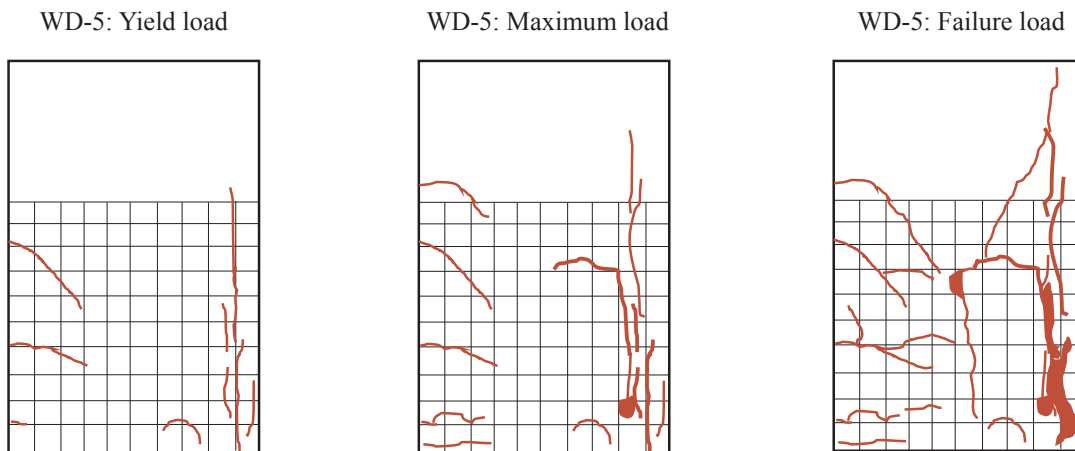
$$M = N\Delta + VH \quad (1)$$

where N is the axial load, Δ is the displacement, V is the shear force, and H (listed in Table 4) is the total height of the column considering the spherical hinge.

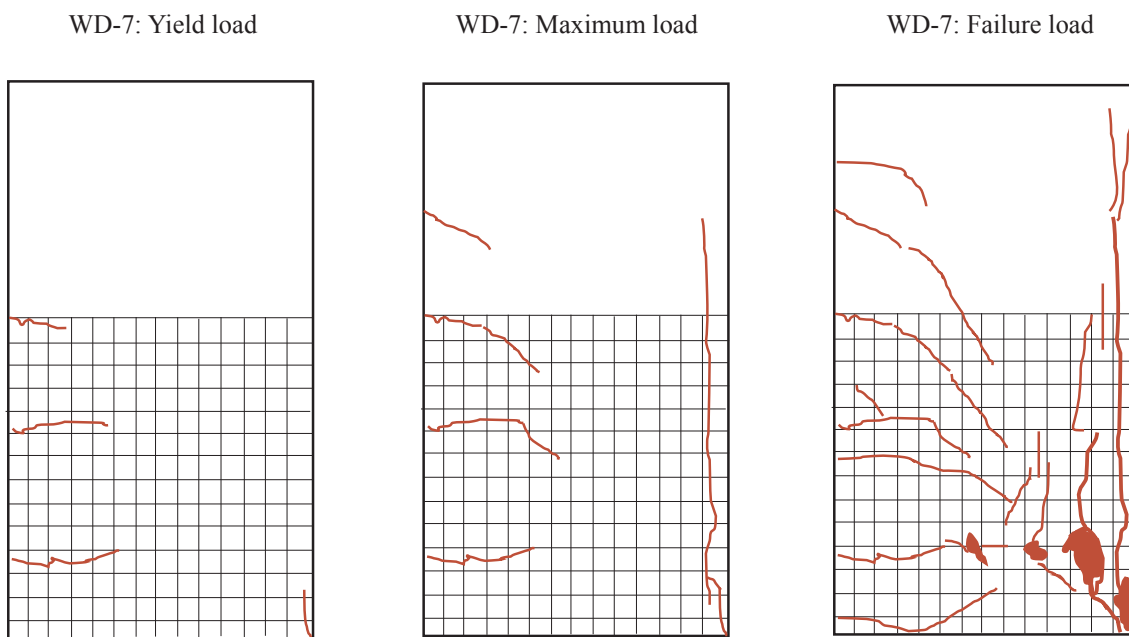
The ratio of M to $f_{ck}bh_0^2$ was used to gage the relative nominal flexural strength [26]. The relationship of the relative nominal flexural strength to the nominal angle of rotation is shown in Fig. 14, which reflects the size effect on the relative nominal flexural strength. The nominal angle of rotation is given by Δ/H_0 , where Δ is the displacement of the column and H_0 is the theoretical height of the column. It can be seen in the figure that the relative nominal flexural strength exhibits a size effect in the maximum load and softening stages. The effect of section size on the relative nominal flexural strength at the maximum load is shown in detail in Fig. 15. It can be seen that the relative nominal flexural strengths decrease by 33% as the section size increases from smallest to largest, except for the WF-3 specimen, which does not behave in accordance with the trend that suggests a size effect in the other specimens. The cause of this behavior may include two aspects: the effect of the eccentric axial load and the presence of horizontal



(a) Development of failure modes of WD-3 specimen



(b) Development of failure modes of WD-5 specimen



(c) Development of failure modes of WD-7 specimen

Fig. 8. Development of failure modes for monotonic specimens.

torque. Notably, between monotonic and cyclic specimens, the size effect appears to have the same general influence on behavior.

3.4.2. Analysis of energy dissipation capacity

The equivalent viscous-damping ratio was used in this study as an index to evaluate the energy dissipation capacity of the specimens [39], and is defined as the ratio of energy dissipated to the energy produced

by an equivalent elastic body under the same displacement. The formula for the equivalent viscous-damping ratio is given by

$$\xi_{eq} = \frac{1}{2\pi} \frac{S_{(ABC+CAD)}}{S_{(OBE+ODF)}} \tag{2}$$

where $S_{(ABC+CAD)}$ is the area of the hysteresis curve shown in Fig. 16 and $S_{(OBE+ODE)}$ is the sum of triangular area for OBE and ODF , also shown in

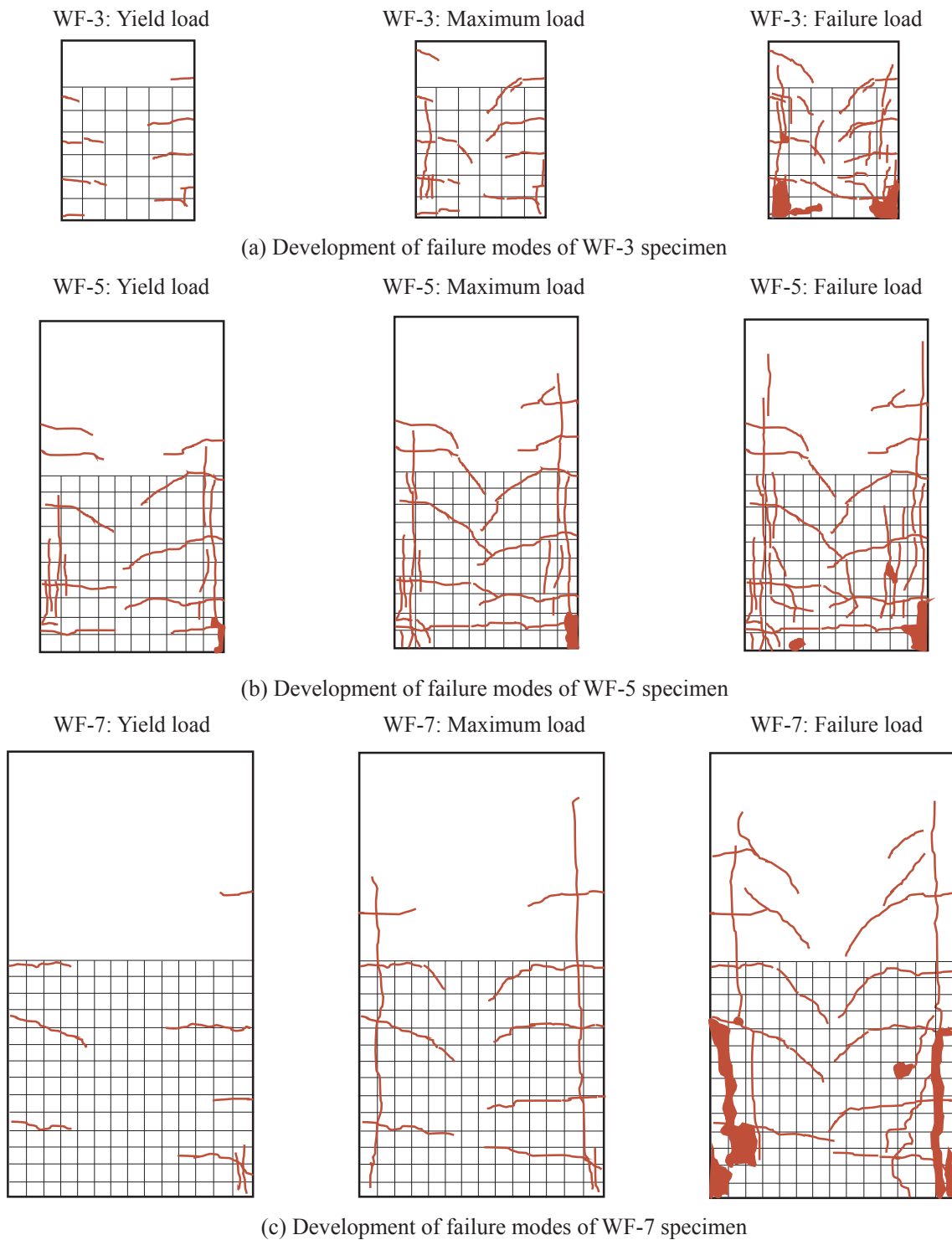


Fig. 9. Development of failure modes for cyclic specimens.

Fig. 16.

The relationship between the equivalent viscous-damping ratio and the nominal angle of rotation is shown in Fig. 17, in which it can be seen that the equivalent viscous-damping ratio increases as the nominal angle of rotation increases, indicating that the energy dissipation capacity increases gradually with deflection. However, the equivalent viscous-damping ratios shown in Fig. 17 can't reflect the effect of section size on the energy dissipation capacity due to the effect of the nominal angle of rotation because the nominal angle of rotation decreases by 42% as the section size increases from smallest to largest

under maximum load.

In order to evaluate the effect of section size on energy dissipation, the average energy dissipation coefficient proposed by Liang [42] was used as the evaluation index, given by

$$\mu_e = \frac{E}{mE_y} \tag{3}$$

where E is the total hysteresis loop area from yield load to failure load (85% of the maximum sustained load); $E_y = P_y \Delta_y / 2$ is the equivalent elastic energy; P_y and Δ_y are the yield load and yield displacement,

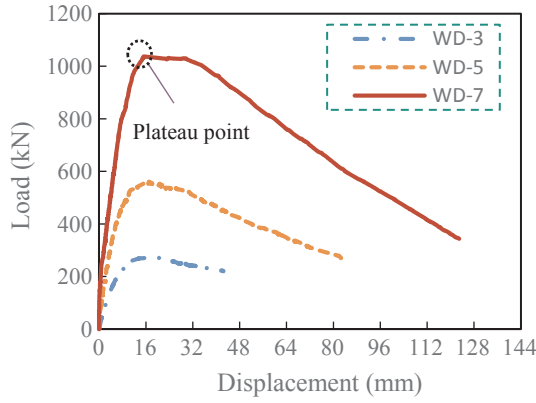


Fig. 10. Load-displacement curves for monotonic specimens.

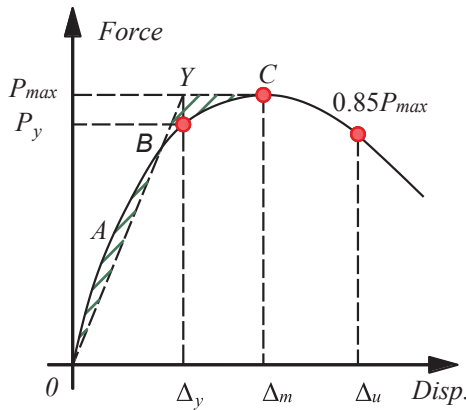


Fig. 11. Calculation of characteristic points.

Table 5
Values of load and displacement for WD specimens.

Test no.	Yield		Maximum		Failure	
	P_y [kN]	Δ_y [mm]	P_m [kN]	Δ_m [mm]	P_u [kN]	Δ_u [mm]
WD-3	240.8	8.83	271.9	17.8	230.9	37.31
WD-5	482.4	8.68	560.4	17.0	476.4	38.43
WD-7	874.6	9.54	1037.0	15.3	881.5	48.38

respectively; and m is the total number of cycles from yield load to failure load. The resulting average energy dissipation coefficients for the different size specimens are shown in Fig. 18, in which it can be seen that the average energy dissipation coefficient decreases by 43% as the section size increases from smallest to largest. Thus, these results prove the existence of an obvious size effect.

4. Effect of section size on moment capacity

4.1. Theoretical calculation of moment capacity

(1) Chinese Code for Design of Concrete Structures [43]

It can be seen in Tables 7 and 8 that the strain in the tensile longitudinal bars reaches the yield point due to bending, the strain in the compressive longitudinal bars reaches the yield point due to the combined action of the axial load and bending, but the stirrups never reach the yield point. This behavior conforms to the general moment capacity calculation method. A simple diagram for calculating moment capacity is shown in Fig. 19. According to the balance of axial forces and moment about the centerline of the section, the equations for axial force (N) and moment (M) are

$$N = \alpha_1 f_{ck} bx + f'_{yk} A'_s + \sigma'_1 A'_s - \sigma_1 A_s - f_{yk} A_s \quad (4)$$

$$M_c = Ne + VH = \alpha_1 f_{ck} bx \left(\frac{h}{2} - \frac{x}{2} \right) + \frac{1}{2} \sigma'_1 A'_s P_0 + 2f'_{yk} A'_s \left(\frac{h}{2} - a'_s \right) + \frac{1}{2} \sigma_1 A_s P_0 \quad (5)$$

and the stress in the longitudinal bars that have not yet reached the yield point is given by

$$\sigma_s = E_s \varepsilon_{cu} \left(\frac{\beta_1 (h_0 - P_0)}{x} - 1 \right) \quad (6)$$

$$\sigma'_s = E_s \varepsilon_{cu} \left(1 - \frac{\beta_1 (P_0 + a'_s)}{x} \right) \quad (7)$$

where α_1 is the ratio of the force in the equivalent rectangular compressive stress block to the axial compressive strength; β_1 is the ratio of the depth of equivalent rectangular compressive stress block to the distance from the neutral axis to the fiber of maximum compressive strain; P_0 is the spacing between the longitudinal bars, which is uniform; ε_{cu} is the ultimate compressive strain; x is the depth of the equivalent rectangular compressive stress block; a'_s is the distance from the compressive longitudinal bar to the compressive face; a_s is the distance from the tensile longitudinal bar to the tensile face; E_s is the modulus of elasticity; f_{yk} and f'_{yk} are the yield strength of the longitudinal tension and compression bars, respectively; A_s and A'_s are the cross-sectional areas of the longitudinal tension and compression bars, respectively; f_{ck} is the axial compressive strength; e is the eccentric distance from the line of axial load application to the centerline of the section; V is the applied horizontal load; and H is the column height including the hinge.

The ratio of the experimentally determined load-bearing capacity to the load-bearing capacity calculated according to the code is defined as the factor of safety of the column. Because the factor of safety is dimensionless, in this paper, it was selected as the evaluation index to reflect the sufficiency of the provided moment capacity. The factor of safety α is defined as M_t/M_c , where M_t is the experimentally determined moment capacity, $M_t = N\Delta + VH$ (in which N is the axial load, Δ is the horizontal displacement, V is the horizontal load, and H is the total height including the hinge), and M_c is the theoretical moment capacity calculated using the Chinese Code as given in Eq. (3). The resulting moments and factors of safety are given in Table 9.

(2) Building Code Requirements for Structural Concrete (ACI 318-14) [44]

Though the equations for the calculation of moment capacity are quite similar, the primary difference between calculating moment capacity with ACI 318-14 and the Chinese code is that the ratio of the equivalent rectangular compressive stress block to the axial compressive strength is set to 0.85 in the ACI Code. Furthermore, the variable β_1 is used to represent the ratio of the depth of the equivalent rectangular compressive stress block to the distance from the neutral axis to the fiber of maximum compressive strain. When $17 \leq f'_c \leq 28$ MPa, $\beta_1 = 0.85$; when $28 < f'_c < 55$ MPa, $\beta_1 = 0.85 - 0.05(f'_c - 28)/7$; and when $f'_c \geq 55$ MPa, $\beta_1 = 0.65$. In the current study, $f_{cu,k} = 67.98$ MPa and $f'_c = 0.79f_{cu,k} = 53.7$ MPa. Therefore, $\beta_1 = 0.66$. The resulting moments and factors of safety are provided in Table 10.

The effect of section size on the factor of safety is shown in Fig. 20, in which it can be seen that the factor of safety decreases by 24% as the section size increases from smallest to largest. Notably, the size effect is consistent between codes within the monotonic and cyclic specimen groups. The factor of safety calculated by ACI is slightly larger than that calculated by the Chinese Code. These data effectively confirm that the evaluated design codes are based on a limit state approach, and thus neglect size effects. This leads to potentially unsafe large sized components when they are designed in accordance with these codes. To

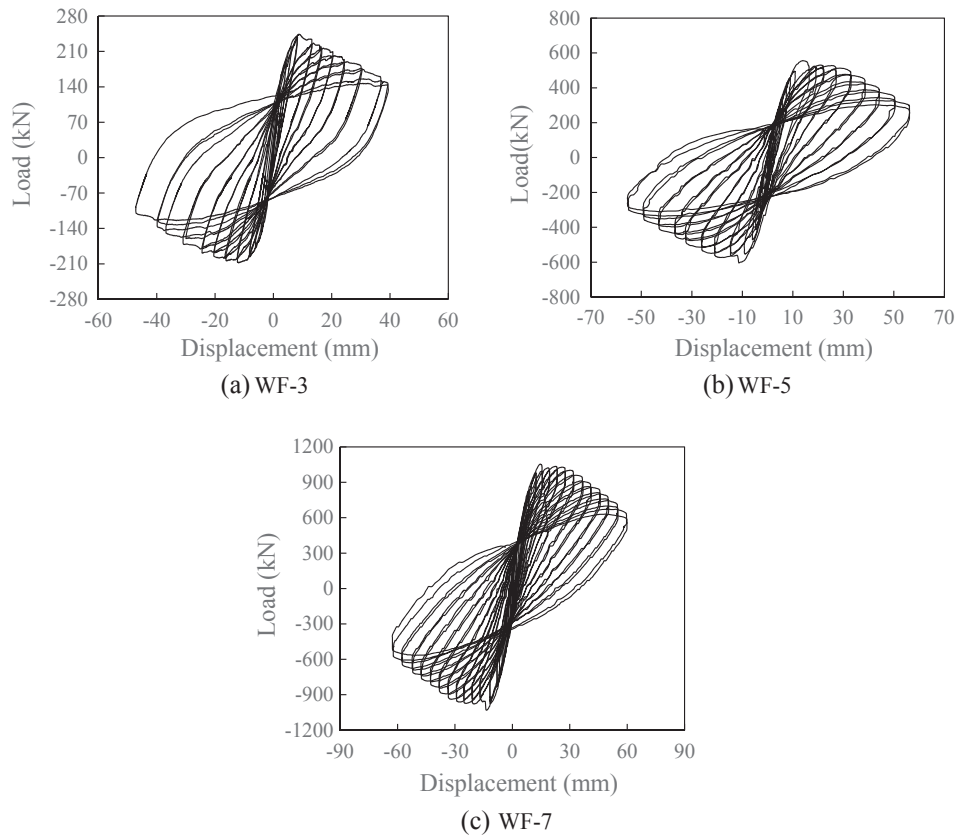


Fig. 12. Hysteresis curves of specimens.

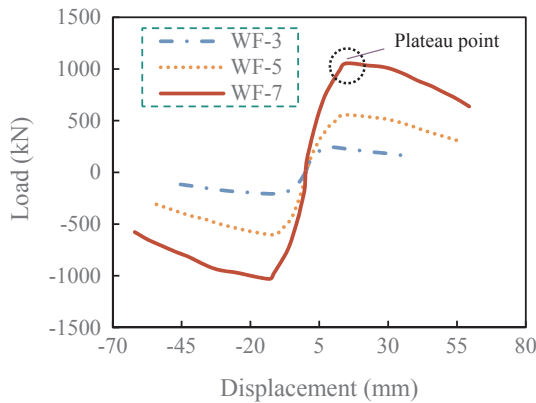


Fig. 13. Skeleton curves of WF specimens.

Table 6
Values of load and displacement for WF specimens.

Test no.	Direction	Yield		Maximum		Failure	
		P_y [kN]	Δ_y [mm]	P_m [kN]	Δ_m [mm]	P_u [kN]	Δ_u [mm]
WF-3-4	Positive	207	5.21	244	8.90	207	21.0
	Negative	182	6.44	208	12.10	176	29.00
WF-5-4	Positive	487	10.40	556	13.80	473	35.40
	Negative	528	7.90	604	11.40	513	29.00
WF-7-4	Positive	921	10.89	1054	14.70	896	40.07
	Negative	882	9.30	1031	13.30	876	37.90

Table 7
Strain in longitudinal reinforcement and stirrups of WD specimens.

Test no.	Load stage	$\epsilon_1 (\times 10^{-6})$	$\epsilon_2 (\times 10^{-6})$	$\epsilon_z (\times 10^{-6})$	$\epsilon_g (\times 10^{-6})$
WD-3	Maximum load	4805(21.5)	2429	62(43)	1752
				147(86)	
WD-5	Maximum load	2332(35.5)	2310	659(71)	1779
				781(142)	
WD-7	Maximum load	-(50.0)	2374	107(100)	1736
				201(200)	

Notes: ϵ_1 and ϵ_2 represent the measured strain in the longitudinal bars and stirrups, respectively; ϵ_z and ϵ_g represent the yield strain in the longitudinal bars and stirrups, respectively; the number inside the parentheses represents the distance from the foot of the column to the strain gage location (in mm); and “-” represents no value.

Table 8
Strain in longitudinal reinforcement and stirrups of WF specimens.

Test no.	Load stage	$\epsilon_3 (\times 10^{-6})$	$\epsilon_z (\times 10^{-6})$	$\epsilon_4 (\times 10^{-6})$	$\epsilon_g (\times 10^{-6})$
WF-3	Maximum load	2531(21.5)	2429	1042(43)	1752
				2199(86)	
WF-5	Maximum load	3345(35.5)	2310	230(71)	1779
				279(142)	
WF-7	Maximum load	2463(250)	2374	1702(100)	1736
				614(200)	

Notes: ϵ_3 and ϵ_4 represent the measured strain in the longitudinal bars and stirrups, respectively; ϵ_z and ϵ_g represent the yield strain in the longitudinal bars and stirrups, respectively; and the number inside the parentheses represents the distance from the foot of the column to the gage location (in mm).

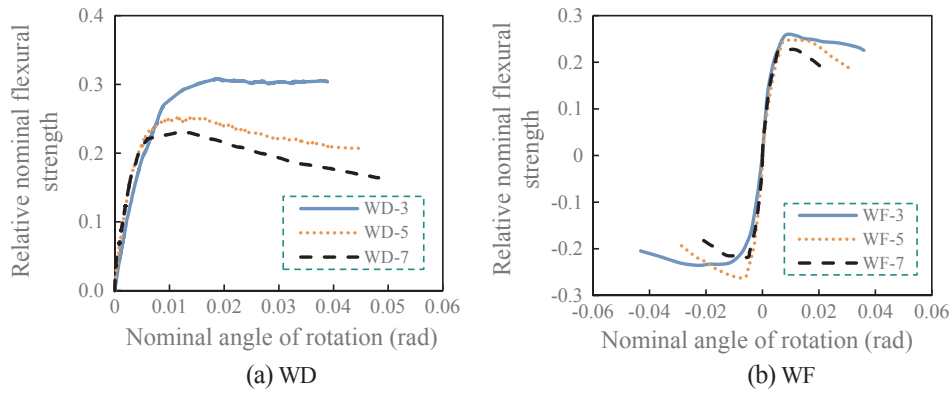


Fig. 14. Relationship of relative nominal flexural strength to the nominal angle of rotation.

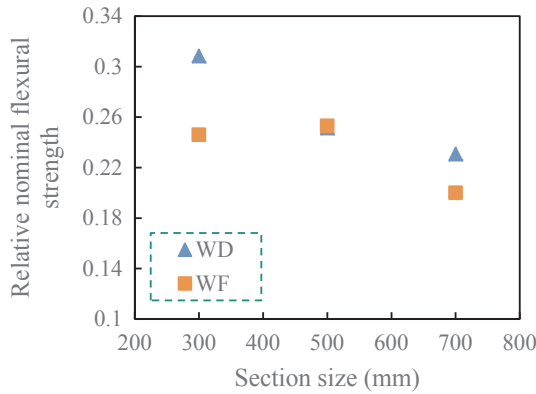


Fig. 15. Relative nominal flexural strength for different section sizes.

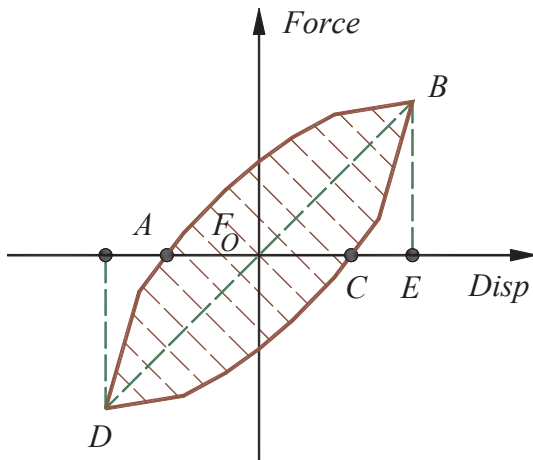


Fig. 16. Calculation of viscous-damping ratio.

address this potentially unsafe design condition, the equations for calculating moment capacity should be modified.

4.2. Size effect analysis based on fracture mechanics

The Type 2 size effect model proposed by Bažant [6] is used in this section as the theoretical model for determining the size effect according to the analysis of failure modes. The Type 2 equation is

$$\alpha_{hd} = Bf_t / \sqrt{1 + h/D_0} \tag{8}$$

where h is the height of the section, B is a dimensionless constant, D_0 is the size at which behavior transitions from ductile to brittle, and f_t is the axial tensile strength of the concrete; in this study, $f_t = 3.76$ MPa.

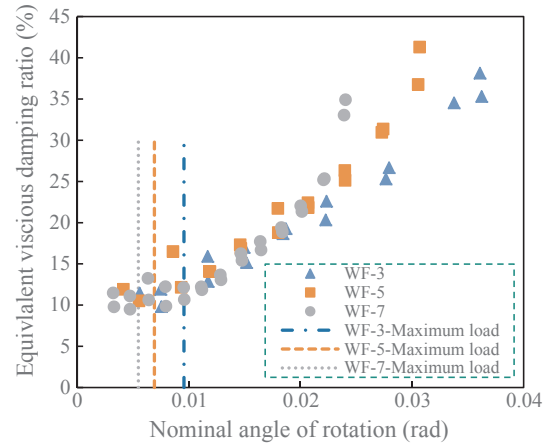


Fig. 17. Relationship between equivalent viscous-damping ratio and nominal angle of rotation.

In order to obtain the two empirical parameters, B and D_0 , Eq. (8) can be rearranged into

$$\left(\frac{f_t}{\alpha_{hd}}\right)^2 = \frac{1}{B^2} + \frac{h}{B^2D_0} \tag{9}$$

which is of the form $Y = AX + C$, where $Y = \left(\frac{f_t}{\alpha_{hd}}\right)^2$, $X = h$, $C = \frac{1}{B^2}$, and $A = \frac{1}{B^2D_0}$. Then B and D_0 can be determined from a regression analysis according to the preceding factor of safety relationships.

For the monotonic and cyclic specimens WD and WF, the equation capturing the size effect in the form of Eq. (8) is therefore

$$\alpha_{hd} = 0.7055f_t / \sqrt{1 + h/195.6} \tag{10}$$

which can also be expressed as

$$\frac{\alpha_{hd}}{Bf_t} = 1 / \sqrt{1 + h/D_0} \tag{11}$$

Li et al. [26] and Xie et al. [28] investigated the effect of member size on the seismic performance of conventional RC columns subjected to monotonic and cyclic loading, finding that the factor of safety exhibits a clear size effect. To confirm this effect in the current study, Fig. 21 shows the relationship between the factor of safety and section size for the conventional C30 RC columns from [26] and [28], as well as the evaluated high-strength C60 RC columns, in which $\text{Log}(h/D_0)$ is plotted against $\text{Log}\left(\frac{\alpha_{hd}}{Bf_t}\right)$. It can be seen that the size effect is stronger in high-strength specimens than in conventional specimens: the response of high-strength concrete to size lies closer to the linear elastic fracture mechanics asymptote (indicated by LEFM), i.e. the column is more brittle. This brittleness has previously been characterized by the

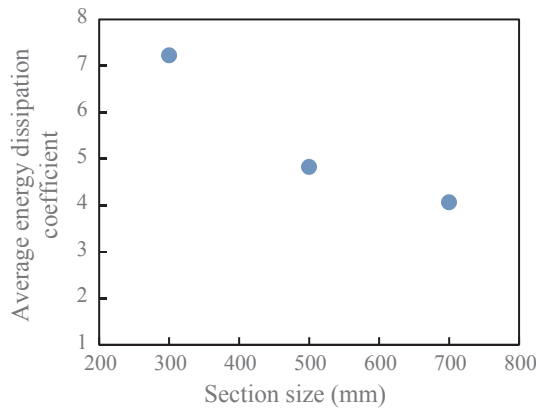


Fig. 18. Relationship between average energy dissipation coefficient and section size.

so-called brittleness number, $\beta = h/D_0$ [45]. It can be seen that the brittleness number of high-strength concrete is larger than that of conventional concrete, indicating that the size effect is more pronounced as the brittleness number increases with the concrete strength.

In order to check the degree of fit of the test results with the Type 2 size effect model proposed by Bažant [6], a correlation coefficient, $\rho_{XY} = \frac{Cov(X,Y)}{\sqrt{D(X)}\sqrt{D(Y)}}$ where $X = h$ and $Y = (1/\alpha_{hD})^2$, was used to evaluate the results. The correlation coefficient for the data collected in study is 0.7. For conventional concrete, the correlation coefficient was 0.76. The correlation coefficients of both types of concrete suggest a very strong correlation between the test results and the Type 2 Bažant model, indicating behavior consistent with the theoretical work of Bažant [6] for both monotonic and cyclic specimens.

4.3. Modification of moment capacity

In order to eliminate the effect of section size on the factor of safety, the Type 2 size effect model was used as a modification coefficient to improve the moment capacity calculated by the Chinese Code [43]. In many metals, the strength is not influenced by any size effect [45]. Therefore, only the moment capacity of concrete share of column resistance should be modified using Bažant's Type 2 size effect model. This can be expressed as $\alpha_c \alpha_1 f_{ck} b x (h/2 - x/2)$, where α_c is the size effect parameter.

First, the moment resistance provided by only the concrete is calculated according to the total tested moment capacity, M_{tc} . Then, according to Eq. (5), the theoretical moment capacity of the concrete is calculated as M_{cc} . The proportion M_{tc}/M_{cc} is then defined as the local factor of safety. The resulting local factors of safety are provided in Table 11. Fig. 22 describes the relationship between the local factor of safety and the section size, in which it can be seen that the local factor

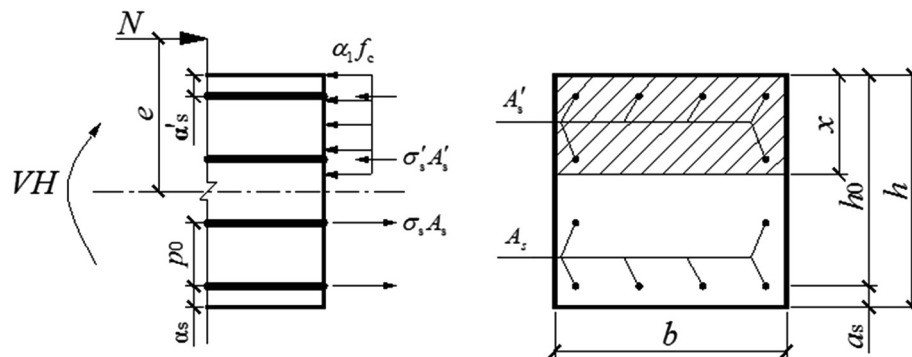


Fig. 19. Moment capacity calculation diagram.

Table 9
Factor of safety calculated using the Chinese Code.

Test no.	M_t [kN·m]	M_c [kN·m]	M_t/M_c
WD-3	342	212.6	1.61
WD-5	1292	970.4	1.33
WD-7	3254	2668.1	1.22
WF-3	274	212.6	1.29
WF-5	1307	970.4	1.35
WF-7	3146	2668.1	1.18

Table 10
Factor of safety calculated using ACI 318-14.

Test no.	M_t [kN·m]	M_c [kN·m]	M_t/M_c
WD-3	342	197	1.74
WD-5	1292	896	1.43
WD-7	3254	2464	1.32
WF-3	274	197	1.39
WF-5	1307	896	1.46
WF-7	3146	2464	1.28

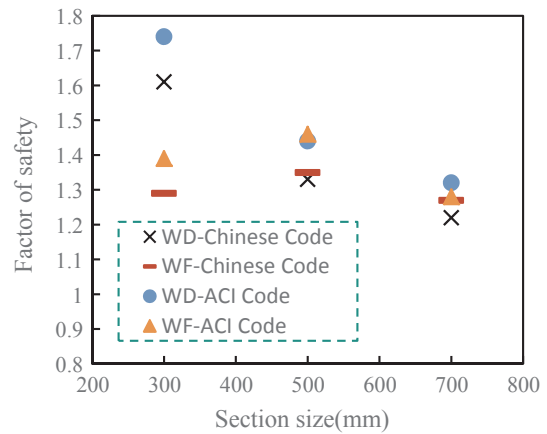


Fig. 20. Comparison of factors of safety determined using different codes for calculating moment capacity.

of safety decreases by 32% as the section size increases from smallest to largest. Furthermore, for both the monotonic and cyclic specimens, the size effect is similar, except for specimen WF-300.

Adopting the same method as applied to the factor of safety, the B and D_0 of the Bažant Type 2 size effect are calculated again. Due to the large error discretization of the WD-3 data, the local factor of safety for this specimen was not considered in the data fitting. Then, for the monotonic and cyclic specimens, the size effect equation can be expressed as

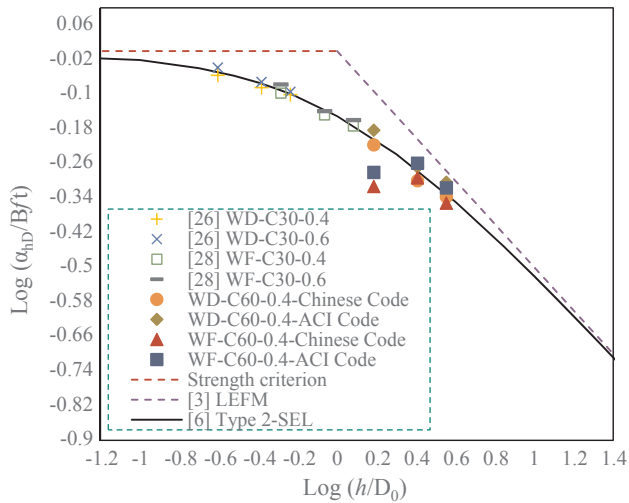


Fig. 21. Comparison of Type 2 size effect model [6], linear elastic fracture mechanics [3], test results of conventional concrete columns from [26] and [28], and test results of high-strength concrete columns from the current study.

Table 11
Local factor of safety calculated by the Chinese Code.

Test no.	M_{tc} [kN·m]	M_{cc} [kN·m]	M_{tc}/M_{cc}
WD-3	285.7	156.4	1.83
WD-5	1045.6	724.1	1.44
WD-7	2572.9	1986.9	1.30
WF-3	217.9	156.4	1.39
WF-5	1060.3	724.1	1.46
WF-7	2466.9	1987.2	1.24

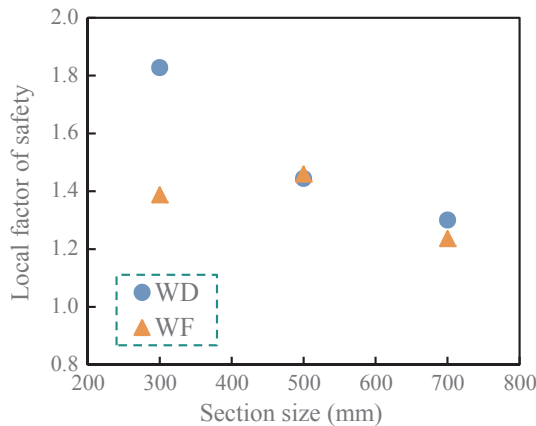


Fig. 22. Local factor of safety for different section sizes.

$$\alpha_c = 1.151f_t / \sqrt{1 + h/64.66} \quad (12)$$

By dividing Eq. (12) by the local factor of safety, the size effect equation can be expressed as

$$\alpha_c = 1.151f_t / \sqrt{1 + h/64.66} / \alpha_{c1} \quad (13)$$

where α_{c1} is the local factor of safety of the minimum section size.

Introducing Eq. (13) into Eq. (4) provides a moment capacity equation accounting for the size effect as follows:

$$M_c = \alpha_c \alpha_{c1} f_{ck} b x \left(\frac{h}{2} - \frac{x}{2} \right) + \frac{1}{2} \sigma_{1s} A_s P_0 + 2f'_{yk} A'_s \left(\frac{h}{2} - a'_s \right) + \frac{1}{2} \sigma_{1s} A_s P_0 \quad (14)$$

Using Eq. (14), the factors of safety were calculated again and are provided in Fig. 23. Clearly, the modified factors of safety tend to be

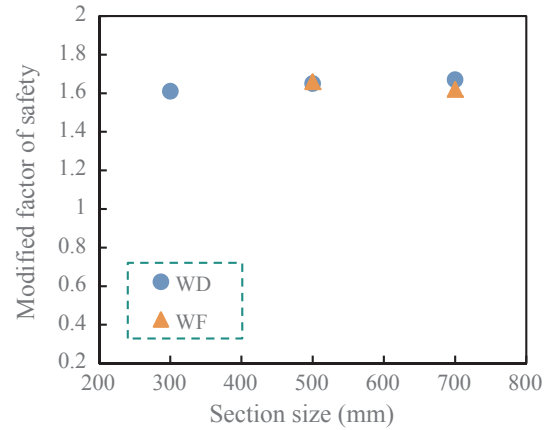


Fig. 23. Modified factor of safety using proposed coefficient based on the Bažant Type 2 size effect.

very constant regardless of size, indicating that the moment capacity of the larger sized specimens will be as safe as those of the smaller sized sections when designed using the proposed Bažant Type 2 size effect coefficient modification.

5. Conclusions

The effects of section size on the seismic performance of high-strength RC columns subjected to monotonic and cyclic loading were experimentally investigated using three different size columns. The results demonstrated the existence of the size effect on the seismic performance of the columns. Some concluding remarks are as follows:

- (1) It was found that the seismic performance of high-strength RC columns exhibits a strong size effect in which the relative nominal flexural strength, average energy dissipation coefficient, factor of safety, and local factor of safety all decreased by 33%, 43%, 24%, and 32%, respectively, as the section size increased from smallest to largest. Moreover, the size effect on the factor of safety for high-strength RC columns was more pronounced than for conventional RC columns.
- (2) The change in factor of safety with size was in good agreement with the Type 2 size effect model proposed by Bažant.
- (3) Based on the test results and the Type 2 size effect model proposed by Bažant, the typical code equation for moment capacity was modified and shown to provide a constant factor of safety regardless of member size.

The experimental results presented in this study should be a valuable addition to the larger research database supporting the study of the size effect on high-strength RC columns subjected to monotonic and cyclic loading. However, it must be noted that the present study mainly concentrated on the size effect with respect to the use of high-strength concrete. A further investigation on the influence of the shear-span ratio, volume-stirrup ratio, strength of stirrup reinforcement, and axial compression ratio on the size effect in high-strength RC columns will be conducted in future.

Acknowledgements

This work was supported by the Science Fund for Creative Research Groups of the National Natural Science Foundation of China (No. 51408378) and Natural Science Foundation of Hebei Province (No. E2015403018). This support is gratefully acknowledged.

Appendix A. Supplementary material

Supplementary data to this article can be found online at <https://doi.org/10.1016/j.engstruct.2018.12.095>.

References

- [1] Li D, Jin L, Du X, et al. Size effect tests of normal-strength and high-strength RC columns subjected to axial compressive loading. *Eng Struct* 2016;109:43–60.
- [2] Bažant ZP, Chen EP. Scaling of structural failure. *Adv Mech* 1999;50(10):593–627.
- [3] Griffith AA. The phenomena of rupture and flow in solids. *Philos Trans R Soc Lond* 1921;221(2):163–98.
- [4] Weibull W. Phenomenon of rupture in solids. *Proc Royal Swedish Inst of Eng Res (Ingenioersvetenskaps Akad Handl)* 1939;153:1–55.
- [5] Weibull W. A statistical distribution function of wide applicability. *ASME J Appl Mech* 1951;18(2):293–7.
- [6] Bažant ZP. Size effect in blunt fracture: concrete, rock, metal. *ASCE J Eng Mech* 1984;110(4):518–35.
- [7] Carpinteri A, Ferro G. Size effects on tensile fracture properties: a unified explanation based on disorder and factuality of concrete microstructure. *Mater Struct* 1994;27(10):563–71.
- [8] Bažant ZP, Lewis G. *Scaling of structural strength*. 2th ed. Oxford: Elsevier; 2005.
- [9] Bažant ZP, Yu Q. Universal size effect law and effect of crack depth on quasi-brittle structure strength. *J Eng Mech* 2009;135(2):78–84.
- [10] Hoover CG, Bažant ZP. Universal size-shape effect law based on comprehensive concrete fracture tests. *ASCE J Eng Mech* 2014;140(3):473–9.
- [11] Sener S. Size effect tests of high strength concrete. *ASCE J Mater Civil Eng* 1997;9(1):46–8.
- [12] Su J, Fang Z. Scale effect on cubic compressive strength of ordinary concrete and high-strength concrete. *J Build Mater* 2013;16(6):1078–81.
- [13] Yang KH, Chung HS, Lee ET, et al. Shear characteristics of high-strength concrete deep beams without shear reinforcement. *Eng Struct* 2003;25:1343–52.
- [14] Yu Q, Bažant ZP. Can stirrups suppress size effect on shear strength of RC beams? *ASCE J Struct Eng* 2011;137(5):607–17.
- [15] Collins MP, Kuchma DA. How safe are our large, lightly reinforced concrete beams, slabs, and footings. *Acı Struct J* 1999;96(4):482–90.
- [16] Jin L, Li D, Du XL. Mechanical behavior and size effect of moderate high-strength RC columns under monotonic and cyclic axial compression. *Eng Struct* 2016;124:269–85.
- [17] Xu CS, Jin L, Ding Z, et al. Size effect tests of high-strength RC columns under eccentric loading. *Eng Struct* 2016;126:78–91.
- [18] Bažant ZP, Kwon YW. Failure of slender and stocky reinforced concrete columns: tests of size effect. *Mater Struct* 1994;27(2):79–90.
- [19] Li ZB, Guo EW, Zhou XY, et al. Seismic behaviors and size effects of large-scale interior beam-column joints of RC frames. *China Civil Eng J* 2012;45(7):39–47.
- [20] Barbhuiya S, Choudhury AM. A study on the size effect of RC beam-column connections under cyclic loading. *Eng Struct* 2015;95:1–7.
- [21] Koç V, Sener S. Size effect in normal- and high-strength concrete with different notches under the axial load. *ASCE J Mater Civil Eng* 2009;21(9):433–45.
- [22] El-Sayed AK, Shuraim AB. Size effect on shear resistance of high strength concrete deep beams. *Mater & Struct* 2016;49(5):1871–82.
- [23] Du XL, Jin L, Li D. A state of the art review on the size effect of concretes and concrete structures (I): concrete materials. *China Civil Eng J* 2017;9(50):28–45. [in Chinese].
- [24] Zhuang WL, Liu ZY, Jiang JS. Earthquake-induced damage analysis of highway bridges in Wenchuan Earthquake and countermeasures. *Chinese J Rock Mech Eng* 2009;28(7):1377–87. [in Chinese].
- [25] Huo LS, Li HN, Xiao SY, et al. Earthquake damage investigation and analysis of reinforced concrete frame structures in Wenchuan earthquake. *J Dalian Univ Technol* 2009;49(5):1–9. [in Chinese].
- [26] Li ZB, Xie YP, Du XL, et al. Experimental study on size effect of seismic behavior for reinforced concrete columns under Monotonic horizontal loading. *J Building Struct* 2013;34(12):77–85. [in Chinese].
- [27] Li ZB, Xie YP, Du XL, et al. Size effect on shear behavior of reinforced concrete short columns. *J Build Struct* 2013;34(12):86–93. [in Chinese].
- [28] Xie YP, Li ZB, Du XL, et al. Experimental study on size effect of seismic behavior for reinforced concrete columns under low cycle reversed loading. *J Build Struct* 2013;34(12):86–93. [in Chinese].
- [29] Azizinamini A, Kuska S, Brungardt P, et al. Seismic behavior of square high-strength concrete columns. *ACI Struct J* 1994;91(3):336–45.
- [30] John H, Thomsen IV, John WW. Lateral load behavior of reinforced concrete columns constructed using high-strength materials. *ACI Struct J* 1994;91(5):605–15.
- [31] Hwang SK, Yun HD. Effects of transverse reinforcement on flexural behaviour of high strength concrete columns. *Eng Struct* 2004;26:1–12.
- [32] Mirza SA, Azizinamini A, Adebar PE, et al. High-strength concrete columns: state-of-the-art. *ACI Struct J* 1997;94(3):323–35.
- [33] Legeron F, Paultre P. Behavior of high-strength concrete columns under cyclic flexure and constant axial load. *ACI Struct J* 2000;97(14):591–601.
- [34] Xiao Y, Wu YT, Shang SP, et al. Experimental and analytical studies on full-scale high-strength concrete columns. *J Southeast Univ* 2002;32(5):746–9. [in Chinese].
- [35] Liu BQ, Bai GL, Zhang GJ. An experimental study on the seismic behavior of high strength reinforced concrete frame columns with high axial compression. *China Civil Eng J* 2005;38(1):45–50. [in Chinese].
- [36] Wang DY, Wang ZY, Smith ST, et al. Seismic performance of CFRP-confined circular high-strength concrete columns with high axial compression ratio. *Constr Build Mater* 2017;134:91–103.
- [37] Ministry of Construction of the People's Republic of China. GB/T 50081-2002, Standard for test method of mechanical properties on ordinary concrete. Beijing: China Architecture & Building Press; 2003 [in Chinese].
- [38] General Administration of Quality Supervision, Inspection and Quarantine of the People's Republic of China. GB/T 228.1-2010, Metallic materials-Tensile testing-Part 1: Method of test at room temperature. Beijing: Standards Press of China; 2010 [in Chinese].
- [39] Ministry of Construction of the People's Republic of China. JGJ/T 101-2015 Specification for seismic test of buildings. Beijing: China Architecture & Building Press; 2015 [in Chinese].
- [40] Foraboschi P. Predictive multiscale model of delayed debonding for concrete members with adhesively bonded external reinforcement. *Compos: Mech Comput Applicat Int J* 2012;3(4):307–29.
- [41] Foraboschi P. Analytical model to predict the lifetime of concrete members externally reinforced with FRP. *Theor Appl Fract Mech* 2015;75:137–45.
- [42] Liang ST, Ding DJ, Qing Lu. Experimental study of earthquake-resistant energy-dissipation and ductility of reinforced concrete column hinge with composite stirrups. *Indust Construct Mag Agency* 1994(11):16–20. [in Chinese].
- [43] Ministry of Construction of the People's Republic of China. GB 50010-2010 Code for design of concrete structures. Beijing: China Architecture & Building Press; 2010 [in Chinese].
- [44] Building Code ASCE. Requirements for structural concrete (ACI 318–14) and commentary (ACI 318R–14) by ACI Committee 318. *J Archit Eng* 2014:8.
- [45] Bažant ZP, Yu Q. Size effect in compression fracture: splitting crack band propagation. *J Eng Mech* 1997;123(123):162–72.